Available online at www.sciencedirect.com
ScienceDirect
Prostaglandins, Leukotrienes and Essential Fatty Acids 76 (2007) 321–329
Prostaglandins Leukotrienes Essential Fatty Acids
www.elsevier.com/locate/plefa

Simultaneous quantification of seven prostanoids using liquid chromatography/tandem mass spectrometry: The effects of arachidonic acid on prostanoid production in mouse bone marrow-derived mast cells ☆

Takanori Hishinuma[a], Kaori Suzuki[a], Masayoshi Saito[a], Hiroaki Yamaguchi[a], Naoto Suzuki[b], Yoshihisa Tomioka[b], Izumi Kaneko[c], Masao Ono[c], Junichi Goto[a,d,*]

[a]*Graduate School of Pharmaceutical Sciences, Tohoku University*
[b]*Faculty of Pharmaceutical Sciences, Josai International University*
[c]*Department of Pathology, Tohoku University Graduate School of Medicine*
[d]*Department of Pharmaceutical Sciences, Tohoku University Hospital*

Received 13 December 2006; received in revised form 23 March 2007; accepted 4 April 2007

Abstract

We have developed a method for the simultaneous estimation of the levels of the prostanoids 6-keto prostaglandin (PG) $F_{1\alpha}$, PGB_2, PGD_2, PGE_2, $PGF_{2\alpha}$, PGJ_2, and thromboxane (TX) B_2 in blood- or serum-containing medium using liquid chromatography-tandem mass spectrometry. These prostanoids and their deuterium derivatives, which were used as internal standards, were subjected to solid-phase extraction using Empore C18 HD disk cartridges and analyzed in the selected reaction-monitoring mode. A linear response curve starting at 10 pg of prostanoid/tube was observed for each prostanoid. The accuracy of the method was demonstrated with samples containing known amounts of the prostanoids. Furthermore, we used this method to analyze the prostanoids produced in mouse bone marrow-derived mast cells stimulated with arachidonic acid, which resulted in the production of PGD_2, PGE_2, $PGF_{2\alpha}$, and TXB_2. The results suggest that this simultaneous quantification method is useful for the analysis of the production of biomedically important prostanoids.

1. Introduction

Prostanoids are bioactive lipid mediators that are synthesized from arachidonic acid (AA) via the arachidonate cascade. These molecules, which play vital roles in a variety of physiological and pathophysiological conditions, are produced in various tissues and cells *in vivo*. Despite their similar molecular structures, prostanoids have different biological effects [1–7]. For example, prostaglandin (PG) E_2 contributes to inflammation and carcinogenesis [6]. On the other hand, PGD_2 induces bronchocontriction, acts as an allergic mediator [7], and functions as a neurotransmodulator of several centrally controlled functions, such as the sleep–wake cycle [8]. Cyclopentenone prostaglandins are dehydration products of either PGD_2 or PGE_2; dehydration of PGD_2 results in the formation of PGJ_2, whereas dehydration of PGE_2 produces PGB_2. There has been significant recent interest in the roles that cyclopente-

☆A part of this research was supported by Grant-in-Aid for Strategic Japanese-Swedish Cooperative Program on "Multidisciplinary Bio" from Japan Science and Technology Agency, Grant-in-Aid for Scientific Research(B) and Exploratory Research from Ministry of Education, Japan.
*Corresponding author. Department of Pharmaceutical Sciences, Tohoku University Hospital, 1-1 Seiryo-machi, Aoba-ku, Sendai 980-8574, Japan. Tel.: +81 22 717 7527; fax: +81 22 717 7545.
E-mail address: jun1goto@mail.tains.tohoku.ac.jp (J. Goto).

0952-3278/$ - see front matter © 2007 Elsevier Ltd. All rights reserved.
doi:10.1016/j.plefa.2007.04.005

none prostaglandins play in cellular proliferation and differentiation [9,10]. Thromboxane (TX) A_2, and PGI_2, which have short half-lives, are automatically converted to TXB_2 [11,15] and 6-keto $PGF_{1\alpha}$ [11], respectively. TXA_2 has aggregatory and vasoconstrictor effects [6,15]. In contrast, PGI_2 has antiaggregatory and vasodilator effects [11]. $PGF_{2\alpha}$ contributes to parturition and bronchocontriction [1,6,7]. In addition, these prostanoids have pathological effects; the abnormalities they produce have been implicated in a wide range of diseases, including diabetic vascular complications [11–15], atherosclerosis [15], allergic asthma [7,16], rheumatoid arthritis [17], and renal diseases [18]. Despite these observations, the mechanisms that contribute to the production of prostanoids have yet to be clarified. Therefore, a reliable microdetermination method would be very useful for investigations of the functions of PGs in these diseases.

The quantification of prostanoids is generally performed using high-performance liquid chromatography (HPLC) together with a radioimmunoassay or enzyme linked immunosorbent assay. These techniques, however, are associated with a variety of problems, including the use of a radioactive compound, complicated procedures, low sensitivities, poor specificities, cross-reactivity, and complicated clean-up procedures to eliminate interfering substances from biological samples. Additionally, these methods are limited to the detection of a single product at a time. Gas chromatography/selected ion monitoring (GC/SIM) is more sensitive and specific than an immunoassay. Moreover, these methods can be used for the simultaneous quantification of prostanoids [19,20]. The GC/SIM technique, however, requires a complicated derivation procedure.

Mass spectrometry (MS) coupled with liquid chromatography (LC) is sufficiently dependable for reliable sample analysis. In particular, liquid chromatography/tandem mass spectrometry (LC/MS/MS) performed using an electrospray ionization (ESI) interface is a powerful technique that allows for highly specific and quantitative measurement of various compounds in a variety of biological samples [21]. Recently, methods for the quantification of AA metabolites using LC/MS/MS have been reported [22–38]. Some of these methods, however, are not suitable for clinical serum samples and medium containing fetal bovine serum (FBS); many of them require that the serum-containing medium be replaced with serum-free medium. In culture-free medium, however, cells may not perform their native functions.

Membrane lipid metabolites, such as prostaglandins, have been characterized as early mediators that influence the activation of bone marrow-derived mast cells (mBMMCs) [39–41] and the onset of allergic inflammation in murine models [42,43]. The application of LC/MS/MS to PG production in mBMMCs may be useful for the pathologic analysis of allergies and inflammatory affections.

In this study, we established a simple and effective simultaneous quantification method for seven prostanoids using simple solid-phase extraction and LC/MS/MS performed in the selected reaction-monitoring (SRM) mode. Moreover, we detailed the extraction steps required to obtain a level of sensitivity that allows the detection of prostanoid production in serum-containing medium. We then measured the effects of AA on prostanoid production in mBMMCs in the presence of FBS.

2. Materials and methods

2.1. Materials

6-Keto $PGF_{1\alpha}$, 6-keto $PGF_{1\alpha}$-d_4, PGB_2, PGB_2-d_4, PGD_2, PGD_2-d_4, PGE_2, PGE_2-d_4, $PGF_{2\alpha}$, $PGF_{2\alpha}$-d_4, PGJ_2, TXB_2, and TXB_2-d_4 were purchased from Cayman Co. (USA). Other solvents and reagents were of the highest quality available. Empore C18 HD disk cartridges (7 mm/3 mL) were purchased from the Industrial and Consumer sector of 3 M (USA). HPLC-grade solvents were obtained from Wako Pure Chemical Industries (Osaka, Japan).

2.2. LC/MS/MS analysis

The LC/MS/MS system was a Quattro II triple–quadrupole tandem mass spectrometer (Micromass, Manchester, UK) equipped with an ESI interface operated in the negative-ion mode. A nanospace SI-1 HPLC system (Shiseido, Tokyo, Japan) was used. Chromatography was performed on a C18 Capcell Pak UG120 column (Shiseido, Tokyo, Japan; 1.5 × 150 mm, 3 μm) using isocratic elution with acetonitrile–water–acetic acid (40:60:0.02, v/v/v) at a flow rate of 100 μL/min. The column was maintained at 40 °C. Column effluent was introduced into the mass spectrometer between 2 and 14 min after injection using a fused silica capillary.

SRM was performed by monitoring the transitions summarized in Table 1. The thickness of the collision gas (argon) was 1.0×10^{-3} mbar. The capillary voltage was −3500 V. Cone voltage and collision energy were optimized for each compound to obtain optimum sensitivity. The source temperature was 160 °C. Peak areas and calibration curves were obtained using the MassLynx program (Micromass, Manchester, UK).

2.3. Cell culture and extraction procedure

mBMMCs were prepared from suspension cell cultures of bone marrow obtained from young C57BL/

6J male mice (Charles River Japan, Yokohama, Japan). mBMMCs were cultured in RPMI1640 medium containing 10% FBS, 100 U/mL penicillin G, 100 μg/mL streptomycin, 1 mM sodium pyruvate, 1x nonessential amino acids (Sigma, St. Louis, MO), 5 ng/mL murine IL-3 (R&D Systems, Minneapolis, MN), and 50 μM 2-mercaptoethanol at 37 °C under a 95%/5% air/CO_2 atmosphere. For the experiments, we used mBMMC populations in which more than 95% of the cells were positive for IgE binding and c-KIT as measured using flow cytometry.

Table 1
Selected reaction monitoring (SRM) transitions for the liquid chromatography/tandem mass spectrometry (LC/MS/MS) determination of prostanoids

Compound	SRM (m/z)	Cone voltage (V)	Collission energy (eV)
6-keto $PGF_{1\alpha}$	369→163	−30	25
6-keto $PGF_{1\alpha}$-d_4	373→167	−30	25
PGB_2	333→175	−50	20
PGB_2-d_4	337→179	−50	20
PGD_2	351→189	−35	20
PGD_2-d_4	355→193	−35	20
PGE_2	351→271	−35	15
PGE_2-d_4	355→275	−35	15
$PGF_{2\alpha}$	353→193	−50	25
$PGF_{2\alpha}$-d_4	357→197	−50	25
PGJ_2	333→189	−30	20
TXB_2	369→195	−40	15
TXB_2-d_4	373→195	−40	15

mBMMCs (1×10^5 cells/200 μL) were cultured with AA (25 μg/mL). After 24 h of incubation, 200 μL of cultured medium was harvested and assayed. To each 200-μL sample of cultured medium, 6-keto $PGF_{1\alpha}$-d_4, PGB_2-d_4, PGD_2-d_4, PGE_2-d_4, $PGF_{2\alpha}$-d_4, and TXB_2-d_4 (1 ng each) were added as internal standards. The sample was adjusted to pH 4.0 with 1 M HCl and was passed through an Empore C18 HD disk cartridge, which was preconditioned with methanol (2 mL) followed by distilled water (2 mL). The cartridge was washed with distilled water (4 mL) and hexane (4 mL), to remove peptides and salts as well as polar and nonpolar interfering substances. 6-Keto $PGF_{1\alpha}$, PGB_2, PGD_2, PGE_2, $PGF_{2\alpha}$, PGJ_2, and TXB_2 were eluted with hexane/ethyl acetate (1:2, v/v, 1 mL) in a siliconized glass tube to avoid absorption by the tube. After evaporating the solvent, the residue was reconstituted in the mobile phase (40 μL), sonicated for 30 s, and filtrated. The sample was then transferred

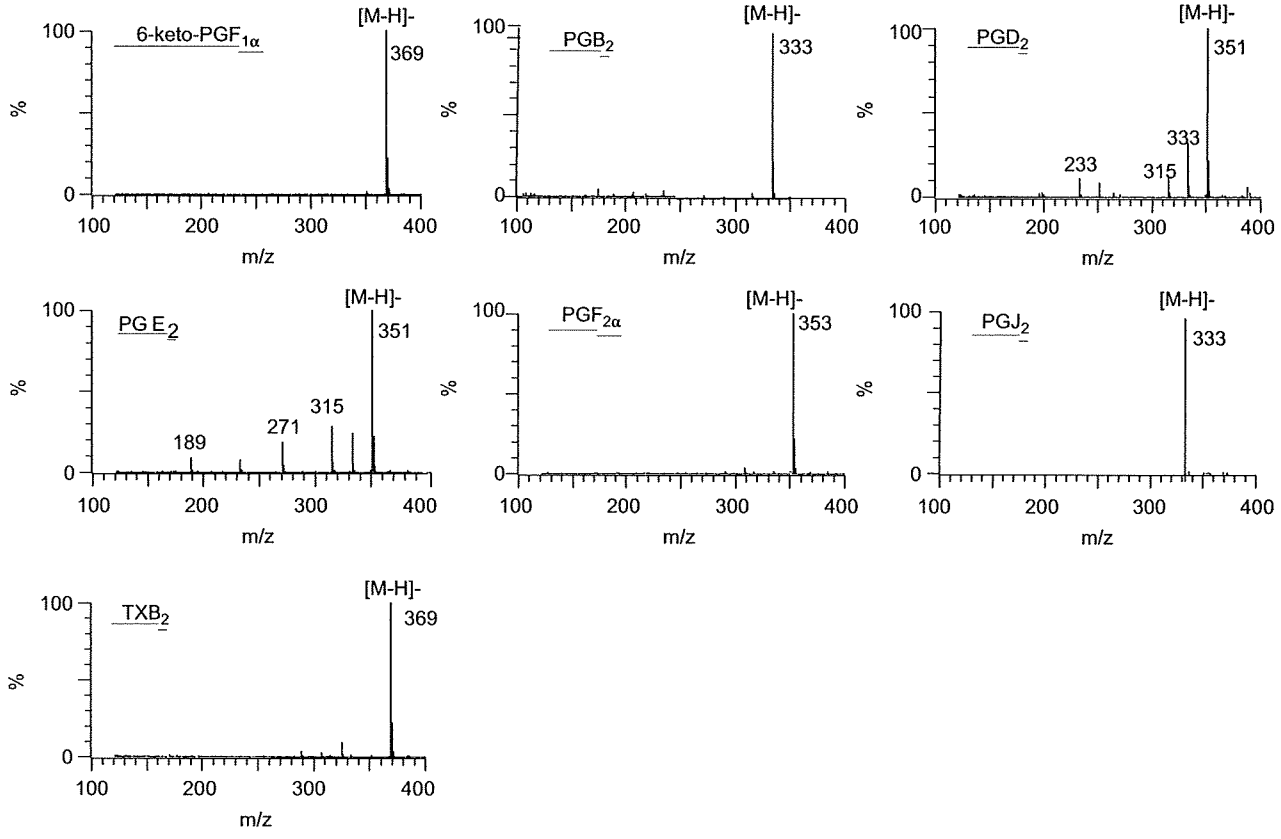

Fig. 1. Mass spectra of the prostanoids.

to an autosampler vial, and 10 μL was injected for LC/MS/MS.

3. Results

3.1. Mass and product ion mass spectra

The mass spectra of 6-keto $PGF_{1\alpha}$, 6-keto $PGF_{1\alpha}$-d_4, PGB_2, PGB_2-d_4, PGD_2, PGD_2-d_4, PGE_2, PGE_2-d_4, $PGF_{2\alpha}$, $PGF_{2\alpha}$-d_4, PGJ_2, TXB_2, and TXB_2-d_4 were obtained (Fig. 1). Each base peak corresponded to the respective deprotonated molecule ($[M-H]^-$). Because prostanoids contain free carboxylic acid groups, ESI results in abundant carboxylate ions. The product ion mass spectra of both the analyte and its internal standard were obtained by choosing the deprotonated molecules as the precursor ions (Fig. 2). Table 1 shows the optimal cone voltage, collision energy, and ion pairs selected for LC/MS/MS determination of each of the compounds.

3.2. Selected reaction-monitoring

In addition to affecting separation on LC, changes in the mobile phase composition can alter the sensitivity of MS by influencing the ionization efficiency of 6-keto $PGF_{1\alpha}$, PGB_2, PGD_2, PGE_2, $PGF_{2\alpha}$, PGJ_2, or TXB_2. Therefore, we first needed to optimize the mobile phase to obtain a high degree of sensitivity, good separation, and a short analysis time. A high degree of sensitivity on MS was concurrently observed with good separation on LC when an acetonitrile/water/acetic acid (40:60:0.02, v/v/v) mobile phase was used. Moreover, this composition also resulted in a short analysis time (Fig. 3).

After optimization of the mobile phase, we tried to detect 6-keto $PGF_{1\alpha}$, PGB_2, PGD_2, PGE_2, $PGF_{2\alpha}$, PGJ_2, and TXB_2 using LC/MS in the selected-ion monitoring (SIM) mode. In the SIM mode, however, attempts to monitor the respective deprotonated molecules for 6-keto $PGF_{1\alpha}$, PGB_2, PGD_2, PGE_2, $PGF_{2\alpha}$, PGJ_2, and TXB_2 failed to produce peaks due to the high background noise level. Therefore, we used LC/MS/MS in the SRM mode. With this method, the background noise level was remarkably reduced and sharp peaks corresponding to 6-keto $PGF_{1\alpha}$, PGB_2, PGD_2, PGE_2, $PGF_{2\alpha}$, PGJ_2, and TXB_2 were observed. Moreover, because we used a semi-micro HPLC system, which included a switching-valve unit to introduce the column effluent for a very brief period of time, only a small sample was required. This meant that the mass spectrometer remained relatively clean and, consequently, the background noise level on the chromatograms was low.

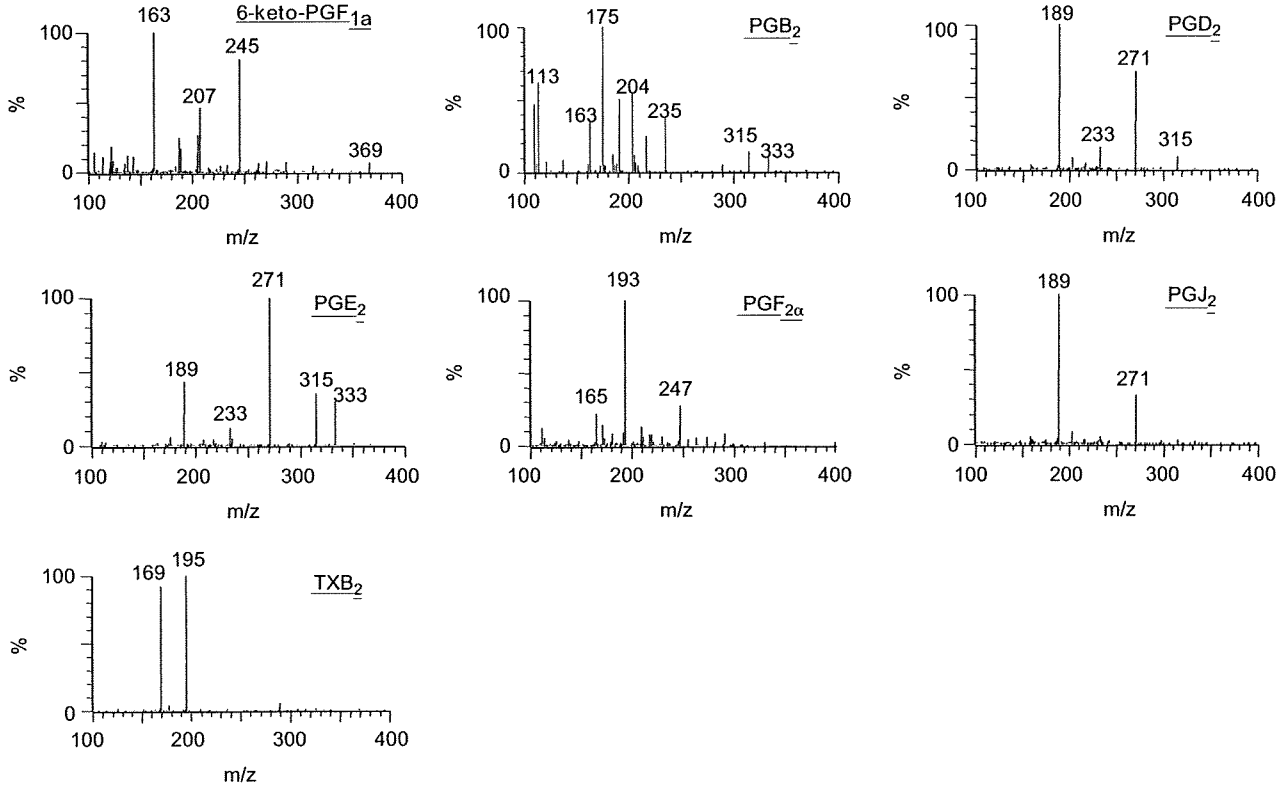

Fig. 2. Product ion mass spectra of the prostanoids.

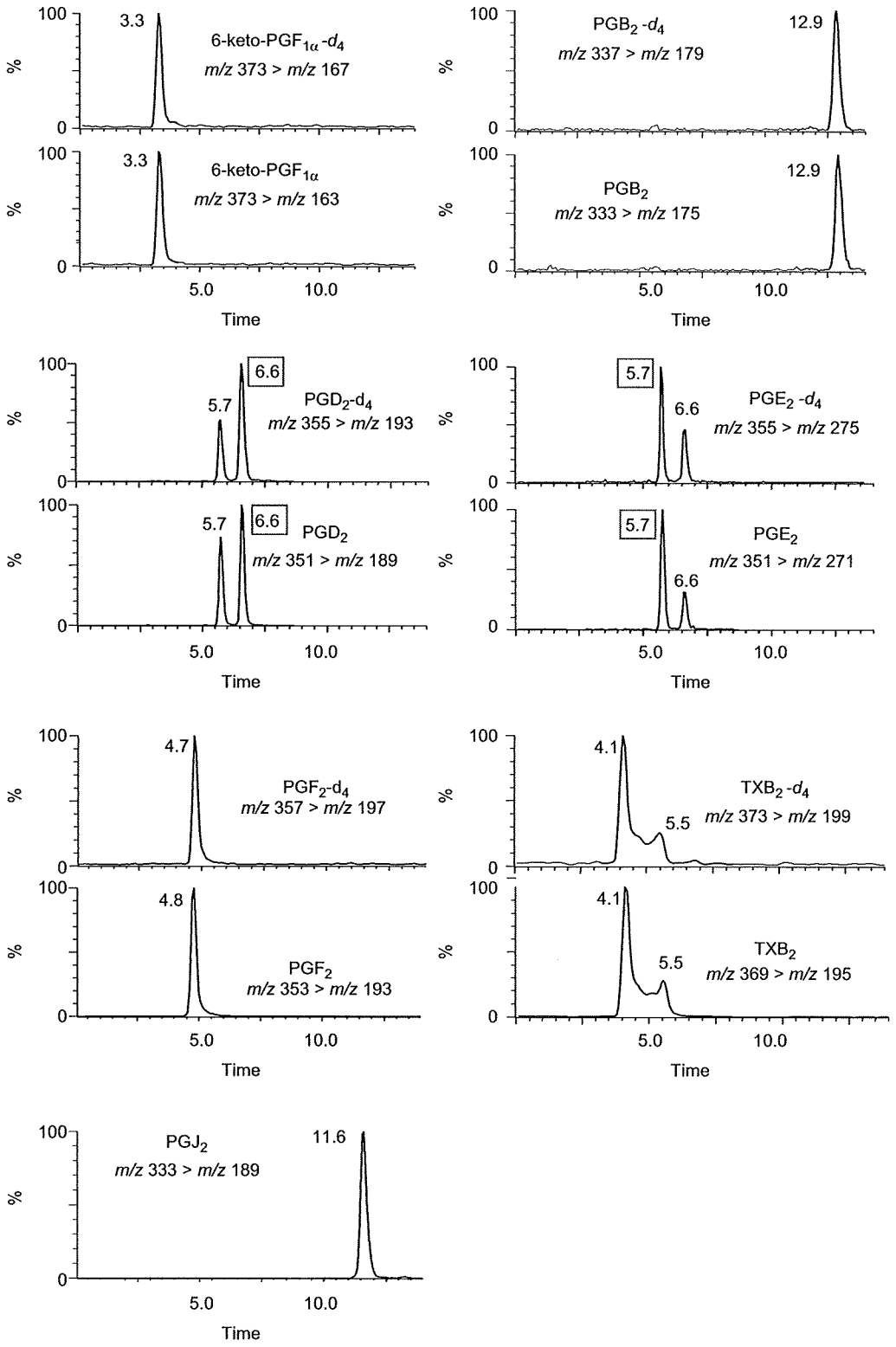

Fig. 3. SRM chromatograms of the prostanoids.

3.3. Calibration curve

A calibration curve for PGE_2 was generated in the SRM using increasing known amounts of PGE_2 and a constant level of PGE_2-d_4 as the internal standard (1). Calibration standards were prepared in triplicate. A linear calibration curve was constructed using least-squares regression quantities vs. the ratio of the peak area to that of the peak corresponding to PGE_2-d_4. 6-keto $PGF_{1\alpha}$, PGB_2, PGD_2, $PGF_{2\alpha}$, and TXB_2 were analyzed using the same method. PGB_2-d_4 was used as an internal standard for the quantitation of both PGB_2 and PGJ_2, because these molecules display similar chromatographic behaviors. The curves for these PGs were relatively linear in the range from 10 pg/tube to 10 ng/tube ($r = 0.999$).

3.4. Accuracy

After the addition of an internal standard to the cell culture medium, three samples were subjected to the sample preparation procedure to demonstrate the experimental reproducibility (Table 2). Statistical analysis was carried out using one-way analysis of variance [44] to separate the analytical errors arising from two sources: sample preparation and LC/MS/MS in the SRM mode. As shown in Table 3A, there was no significant contribution to the total variance from the sample preparation, whereas the coefficient of variation for LC/MS/MS in the SRM mode was 0.66%.

To examine the accuracy and the precision of the present method, cell culture medium spiked with 100, 200, 300, 500, or 1000 pg/tube was prepared. These samples were analyzed in triplicate. The results for PGE_2 are shown in Table 2. The accuracy of the measurements of the added prostanoids ranged between 98.7% and 104%. The coefficients of variation of the analyses of the prostanoids at 100, 200, 300, 500, or 1000 pg/tube ranged from 0.14% to 3.3%, whereas the absolute recovery level of the prostanoids ranged from 80.3% to 95.7%. Statistical analysis was carried out using two-way analysis of variance [44] to separate the analytical errors between sources: sample preparation and LC/MS/MS in the SRM mode. The findings indicate that there was no significant contribution to the total variance from spiking errors or sample preparation (Table 3B). Almost all of the variance in these experiments was attributed to LC/MS/MS in the SRM mode, because the errors from sample preparation and the concentrations of the prostanoids were negligible. These findings suggested that this simultaneous quantification method is highly reliable with good accuracy and precision.

Table 2
Accuracy of PGE_2 spiked cell culture media

	Mean level (pg/2 mL, $n = 3$)	Accuracy (%)	C.V. (%)
Non-spiked	Not detected		
+ 100 pg	100 ± 1.7	101 ± 1.7	1.69
+ 200 pg	201 ± 0.94	100 ± 0.47	0.470
+ 300 pg	300 ± 1.7	99.9 ± 0.57	0.567
+ 500 pg	501 ± 2.5	100 ± 0.50	0.498
+ 1000 pg	1001 ± 2.1	100 ± 0.21	0.205

Table 3
Analysis of variance

Source	S	f	V	F_0
(A) *Analysis of variance from the reproducibility test*				
Sample preparation	20.0	3	6.68	2.20
LC/MS/MS	24.3	8	3.03	–
Total	44.3	11	–	–
$F(3,8,0.05) = 4.07$				
(B) *Analysis of variance from the accuracy test*				
Spiking error (a)	3.98	4	0.955	0.955
Sample preparation (b)	3.87	2	1.94	1.94
a × b	23.2	8	2.90	2.90
LC/MS/MS	30.0	30	1.00	–
Total	61.0	44	–	–
$F(4,30,0.05) = 2.690$				
$F(2,30,0.05) = 3.316$				

S = residual sum of squares; F = number of degrees of freedom; $f_1 = f$ sample preparation; $f_2 = f$ error; V = unbiased variance; F_0 = observed value following F distribution variance ratio (v sample preparation/V error); $F(f_2,F_1,\alpha)$ = density function of F distribution with f_1 and f_2 degrees of freedom.

3.5. Application to cell culture medium

We investigated the production of prostanoids in the mBMMCs in the presence of 25 μg/mL AA (Fig. 4). The mBMMCs without added AA produced $PGF_{2\alpha}$ and TXB_2. The levels of these prostanoids, however, significantly increased following the addition of AA ($p < 0.05$). After the mBMMCs were incubated for 24 h in the presence of AA, the levels of the detected prostanoids were as follows: $TXB_2 > PGD_2 > PGE_2 \approx PGF_{2\alpha}$. 6-Keto $PGF_{1\alpha}$, PGB_2, and PGJ_2 were not detected.

4. Discussion

MS is a powerful technique that can provide highly specific and quantitative measurements of low levels of endogenous biological substances. Recently, LC coupled with MS has been successfully used for pharmaceutical analyses and quantification, because LC/MS combines the separation of the analytes on a LC column and the detection of ions using a mass

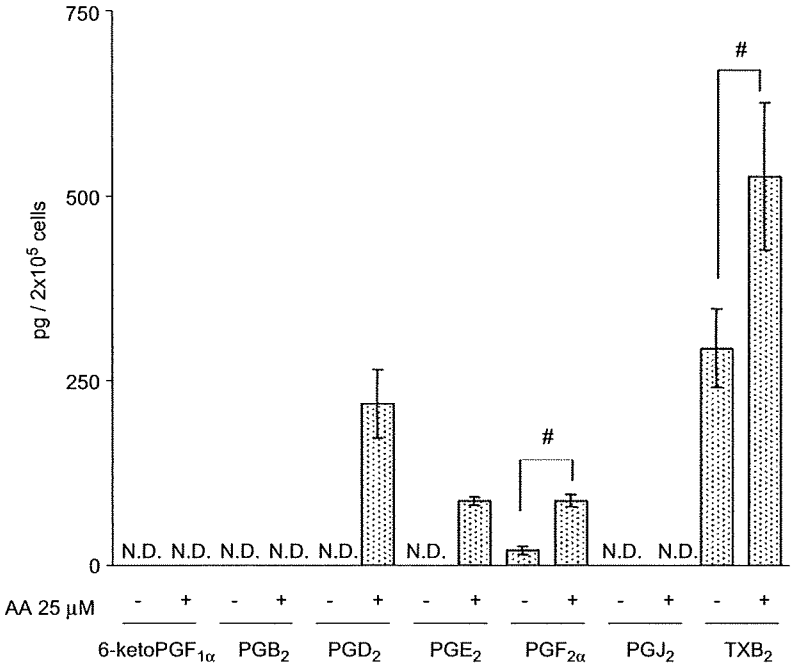

Fig. 4. Effect of AA on prostanoid production in mBMMCs. The mBMMCs (1×10^6 cells/mL) were cultured with AA (25 μg/mL). After 24 h of incubation, 200 μL of medium was harvested and assayed. 6-Keto $PGF_{1\alpha}$-d_4, PGB_2-d_4, PGD_2-d_4, PGE_2-d_4, $PGF_{2\alpha}$-d_4, and TXB_2-d_4 (1 ng each) were added to each 200-μL sample of cultured medium as internal standards. Prostanoids were extracted using Empore C18 HD disk cartridges and analyzed using LC/MS/MS as described in the Materials and Methods section.

spectrometer. For the determination of a wide variety of nonvolatile or thermally labile molecules, such as prostanoids, LC/MS and LC/MS/MS are especially useful. In addition, because of its sensitivity and specificity, LC/MS/MS is well suited for the analysis of prostanoids. With the SRM mode, it is possible to choose and monitor specific fragment ions for each prostanoid to identify and quantify the substrate more sensitively and specifically.

Microdetermination methods for eicosanoids using LC/MS/MS have been reported previously [23–38]. In the present study, we have developed a method for the simultaneous analysis of 6-keto $PGF_{1\alpha}$, PGB_2, PGD_2, PGE_2, $PGF_{2\alpha}$, PGJ_2, and TXB_2 using LC/MS/MS after a simple solid-phase extraction step to clean up the samples. An Empore C18 disk cartridge was used for the extraction of 6-keto $PGF_{1\alpha}$, PGB_2, PGD_2, PGE_2, $PGF_{2\alpha}$, PGJ_2 and TXB_2 from 200 μL of serum-containing medium. Before loading, the sample was acidified to increase the recovery rate by increasing the adsorptive activity. After the sample was loaded, the cartridge was washed with H_2O and hexane. This procedure, together with the use of minimal volumes of washing solvents, produced excellent clean-up results. This cartridge, which yielded good recovery even when a high flow rate was used during the sample loading and washing periods, required as little as 1 mL of elution solvent. Therefore, the time-consuming solvent evaporation step may be unnecessary. This feature is even more important for thermally labile compounds. Moreover, these methods can be used to clean up not only cell culture media, but also biological fluids. We have analyzed prostanoids in human sera and aqueous humor using these methods (data not shown). When tetradeuterium analogues were used as internal standards for each analyte, the present simultaneous quantification method was found to be highly accurate and precise. In the SRM chromatogram, the analyte peaks were well separated, indicating different retention times on the LC column, and no serious interfering peaks were detected. The analyte peaks were detected with retention times that were similar to those of their corresponding internal standards. Additionally, this good separation only required a simple LC system that employed an isocratic elution step. Therefore, our simultaneous quantification method, which has a fixed ionization efficiency, is more simple and reliable and than other previously published methods.

Calibration curves ranging from 10 pg/tube to 10 ng/tube exhibited good linearity. This range covered the levels of prostanoids produced by mBMMCs (2×10^5 cells). We found that mBMMCs without added AA produced $PGF_{2\alpha}$ and TXB_2. After a 24-h incubation in the presence of AA, however, the mBMMCs produced a variety of prostanoids ($TXB_2 > PGD_2 > PGE_2 \approx PGF_{2\alpha}$). In contrast, 6-keto $PGF_{1\alpha}$, PGB_2, and PGJ_2 were not

detected. Across the board, the levels we observed in these experiments were lower than those reported in other studies. This observation may be associated with the ages of the mBMMCs from the various studies. Activated mast cells produce a variety of chemical mediators. Among them, PGD_2 has been reported to be the major cyclooxygenase metabolite of AA, which is produced in response to a diverse range of stimuli [45,46]. A previous study reported that activated rat mast cells generate 6-keto $PGF_{1\alpha}$, PGD_2, PGE_2, $PGF_{2\alpha}$, and TXB_2 [47]. The finding that nonstimulated mBMMCs produce $PGF_{2\alpha}$, but not PGD_2 and PGE_2, however, is novel. The physiological roles of the production of prostanoids by mBMMCs should be elucidated in future studies. Our results suggest that this method will be useful for the investigation of prostanoid production by mBMMCs.

In conclusion, we have developed a rapid, highly specific, and highly sensitive LC/MS/MS-based method for the analysis of prostanoids in cell culture medium. This simultaneous quantification method is effective for the analysis of seven biologically important prostanoids and may be helpful for investigations of the mechanisms of prostanoid production. Because prostanoids have been implicated in numerous pathophysiological conditions, this method may also be of use in a variety of clinical settings.

References

[1] R.J. Helliwell, L.F. Adams, M.D. Mitchell, Prostaglandin synthases: recent developments and a novel hypothesis, Prostaglandins Leukot Essent. Fatty Acids 70 (2004) 101–113.

[2] R.J. Soberman, P. Christmas, The organization and consequences of eicosanoid signalling, J. Clin. Invest. 111 (2003) 1107–1113.

[3] C.D. Funk, Prostaglandins and leukotrienes: advances in eicosanoid biology, Science 294 (2001) 1871–1875.

[4] W.L. Smith, The eicosanoids and their biochemical mechanisms of action, Biochem. J. 259 (1989) 315–324.

[5] P. Needleman, J. Turk, B.A. Jakschik, A.R. Morrison, J.B. Lefkowith, Arachidonic acid metabolism, Annu. Rev. Biochem. 55 (1986) 69–102.

[6] W.L. Smith, R. Langenbach, Why there are two cyclooxygenase isozymes, J. Clin. Invest. 107 (2001) 1491–1495.

[7] L. Pang, A. Pitt, D. Petkova, A.J. Knox, The COX-1/COX-2 balance in asthma, Clin. Exp. Allergy 28 (1998) 1050–1058.

[8] Y. Urade, T. Tanaka, N. Eguchi, M. Kikuchi, H. Kimura, H. Toh, O. Hayaishi, Structural and functional significance of cysteine residues of glutathione-independent prostaglandin D synthase. Identification of Cys65 as an essential thiol, J. Biol. Chem. 270 (1995) 1422–1428.

[9] M. Fukushima, Biological activities and mechanisms of action of PGJ2 and related compounds: an update, Prostaglandins Leukot Essent. Fatty Acids 47 (1992) 1–12.

[10] R. Chinery, R.J. Coffey, R. Graves-Deal, S.C. Kirkland, S.C. Sanchez, W.E. Zackert, J.A. Oates, J.D. Morrow, Prostaglandin J_2 and 15-deoxy-delta12,14-prostaglandin J_2 induce proliferation of cyclooxygenase-depleted colorectal cancer cells, Cancer Res. 59 (1999) 2739–2746.

[11] T. Hishinuma, Y. Koseki, Y. Murai, J. Kotake, F. Ishii, K. Suzuki, M. Mizugaki, Elevation of the thromboxane A_2/prostacyclin ratio in urine of diabetic mice analyzed by gas chromatography/selected ion monitoring, Prostaglandins 55 (1998) 83–93.

[12] T. Hishinuma, Y. Koseki, Y. Murai, T. Yamazaki, K. Suzuki, M. Mizugaki, Urinary thromboxane A_2/prostacyclin balance reflects the pathological state of a diabetic, Prostaglandins Other Lipid Mediat. 58 (1999) 263–271.

[13] T. Hishinuma, H. Tsukamoto, K. Suzuki, M. Mizugaki, Relationship between thromboxane/prostacyclin ratio and diabetic vascular complications, Prostaglandins Leukot Essent. Fatty Acids 65 (2001) 191–196.

[14] M. Nishikawa, T. Hishinuma, K. Nagata, Y. Koseki, K. Suzuki, M. Mizugaki, Effects of eicosapentaenoic acid (EPA) on prostacyclin production in diabetics: GC/MS analysis of PGI_2 and PGI_3 levels, Methods Find. Exp. Clin. Pharmacol. 19 (1997) 429–433.

[15] M. Cocozza, T. Picano, U. Oliviero, N. Russo, V. Coto, M. Milani, Effects of picotamide, an antithromboxane agent, on carotid atherosclerotic evolution. A two-year, double-blind, placebo-controlled study in diabetic patients, Stroke 26 (1995) 597–601.

[16] N. Suzuki, T. Hishinuma, F. Abe, K. Omata, S. Ito, M. Sugiyama, M. Mizugaki, Difference in urinary LTE4 and 11-dehydro-TXB_2 excretion in asthmatic patients, Prostaglandins Other Lipid Mediat. 62 (2000) 395–403.

[17] T. Hishinuma, H. Nakamura, T. Sawai, M. Uzuki, Y. Itabash, M. Mizugaki, Microdetermination of prostaglandin E_2 in joint fluid in rheumatoid arthritis patients using gas chromatography/selected ion monitoring, Prostaglandins Other Lipid Mediat. 58 (1999) 179–186.

[18] T. Hishinuma, Y. Koseki, J. Katayama, Y. Murai, T. Saito, M. Mizugaki, Changes of the thromboxane A2/prostacyclin balance in the urine of patients with renal diseases analyzed by gas chromatography/selected ion monitoring, Prostaglandins Other Lipid Mediat. 60 (2000) 1–8.

[19] H. Tsukamoto, T. Hishinuma, T. Mikkaichi, H. Nakamura, T. Yamazaki, Y. Tomioka, M. Mizugaki, Simultaneous quantification of prostaglandins, isoprostane and thromboxane in cell-culturted medium using gas chromatography-mass spectrometry, J. Chromatogr. B Analyt. Technol. Biomed. Life Sci. 774 (2002) 205–214.

[20] R. Baranowski, K. Pacha, Gas chromatographic determination of prostaglandins, Mini Rev. Med. Chem. 2 (2002) 135–144.

[21] D. Tsikas, Application of gas chromatography-mass spectrometry and gas chromatography-tandem mass spectrometry to assess in vivo synthesis of prostaglandins, thromboxane, leukotrienes, isoprostanes and related compounds in humans, J. Chromatogr. B Biomed. Sci. Appl. 717 (1998) 201–245.

[22] M. Takabatake, T. Hishinuma, N. Suzuki, S. Chiba, H. Tsukamoto, H. Nakamura, T. Saga, Y. Tomioka, A. Kurose, T. Sawai, M. Mizugaki, Simultaneous quantification of prostaglandins in human synovial cell-cultured medium using liquid chromatography/tandem mass spectrometry, Prostaglandins Leukot Essent. Fatty Acids 67 (2002) 51–56.

[23] R.C. Murphy, R.M. Barkley, B.K. Zemski, J. Hankin, K. Harrison, C. Johnson, J. Krank, A. McAnoy, C. Uhlson, S. Zarini, Electrospray ionization and tandem mass spectrometry of eicosanoids, Anal. Biochem. 346 (2005) 1–42.

[24] E. Brewer, J. Henion, Atmospheric pressure ionization LC/MS/MS techniques for drug disposition studies, J. Pharm. Sci. 87 (1998) 395–402.

[25] A. Margalit, K.L. Duffin, P.C. Isakson, Rapid quantitation of a large scope of eicosanoids in two models of inflammation: development of an electrospray and tandem mass spectrometry

method and application to biological studies, Anal. Biochem. 235 (1996) 73–81.
[26] C.S. Newby, A.I. Mallet, Rapid simultaneous analysis of prostaglandin E_2, 12-hydroxyeicosatetraenoic acid and arachidonic acid using high performance liquid chromatography/electrospray ionization mass spectrometry, Rapid Commun. Mass Spectrom. 11 (1997) 1723–1727.
[27] J.A. Hankin, P. Wheelan, R.C. Murphy, Identification of novel metabolites of prostaglandin E_2 formed by isolated rat hepatocytes, Arch. Biochem. Biophys. 340 (1997) 317–330.
[28] E.C. Kempen, P. Yang, E. Felix, T. Madden, R.A. Newman, Simultaneous quantification of arachidonic acid metabolites in cultured tumor cells using high-performance liquid chromatography/electrospray ionization tandem mass spectrometry, Anal. Biochem. 297 (2001) 183–190.
[29] K. Nithipatikom, N.D. Laabs, M.A. Isbell, W.B. Campbell, Liquid chromatographic-mass spectrometric determination of cyclooxygenase metabolites of arachidonic acid in cultured cells, J. Chromatogr. B Analyt. Technol. Biomed. Life Sci. 785 (2003) 135–145.
[30] Y. Kita, T. Takahashi, N. Uozumi, T. Shimizu, A multiplex quantitation method for eicosanoids and platelet-activating factor using column-switching reversed-phase liquid chromatography-tandem mass spectrometry, Anal. Biochem. 342 (2005) 134–143.
[31] R. Schmidt, O. Coste, G. Geisslinger, LC-MS/MS-analysis of prostaglandin E_2 and D_2 in microdialysis samples of rats, J. Chromatogr. B Analyt. Technol. Biomed. Life Sci. 826 (2005) 188–197.
[32] J. Kapron, J. Wu, T. Mauriala, P. Clark, R.W. Purves, K.P. Bateman, Simultaneous analysis of prostanoids using liquid chromatography/high-field asymmetric waveform ion mobility spectrometry/tandem mass spectrometry, Rapid Commun. Mass Spectrom. 20 (2006) 1504–1510.
[33] M. Mizugaki, T. Hishinuma, N. Suzuki, Determination of leukotriene E4 in human urine using liquid chromatography-tandem mass spectrometry, J. Chromatogr. B Biomed. Sci. Appl. 729 (1999) 279–285.
[34] Y. Murai, T. Hishinuma, N. Suzuki, J. Satoh, T. Toyota, M. Mizugaki, Determination of urinary 8-epi-prostaglandin F(2alpha) using liquid chromatography-tandem mass spectrometry: increased excretion in diabetics, Prostaglandins Other Lipid Mediat. 62 (2000) 173–181.
[35] N. Suzuki, T. Hishinuma, T. Saga, J. Sato, T. Toyota, J. Goto, M. Mizugaki, Determination of urinary 12(S)-hydroxyeicosatetraenoic acid by liquid chromatography-tandem mass spectrometry with column-switching technique: sex difference in healthy volunteers and patients with diabetes mellitus, J. Chromatogr. B Analyt. Technol. Biomed. Life Sci. 783 (2003) 383–389.
[36] N. Suzuki, T. Hishinuma, S. Chiba, T. Saga, H. Tsukamoto, M. Mizugaki, J. Goto, Quantitative liquid chromatography-tandem mass spectrometric analysis of 11-dehydro TXB_2 in urine, Prostaglandins Other Lipid Mediat. 73 (2004) 103–110.
[37] P. Yang, D. Chan, E. Felix, T. Madden, R.D. Klein, I. Shureiqi, X. Chen, A.J. Dannenberg, R.A. Newman, Determination of endogenous tissue inflammation profiles by LC/MS/MS: COX- and LOX-derived bioactive lipids, Prostaglandins Leukot Essent. Fatty Acids 75 (2006) 385–395.
[38] P. Araujo, L. Froyland, Optimisation of an extraction method for the determination of prostaglandin E_2 in plasma using experimental design and liquid chromatography tandem mass spectrometry, J. Chromatogr. B Analyt. Technol. Biomed. Life Sci. 830 (2006) 212–217.
[39] B.L. Diaz, H. Fujishima, Y. Kanaoka, Y. Urade, J.P. Arm, Regulation of prostaglandin endoperoxide synthase-2 and IL-6 expression in mouse bone marrow-derived mast cells by exogenous but not endogenous prostanoids, J. Immunol. 168 (2002) 1397–1404.
[40] I. Leal-Berumen, P. O'Byrne, A. Gupta, C.D. Richards, J.S. Marshall, Prostanoid enhancement of interleukin-6 production by rat peritoneal mast cells, J. Immunol. 154 (1995) 4759–4767.
[41] C. Feng, E.M. Beller, S. Bagga, J.A. Boyce, Human mast cells express multiple EP receptors for prostaglandin E_2 that differentially modulate activation responses, Blood 107 (2006) 3243–3250.
[42] S.G. Trivedi, J. Newson, R. Rajakariar, T.S. Jacques, R. Hannon, Y. Kanaoka, N. Eguchi, P. Colville-Nash, D.W. Gilroy, Essential role for hematopoietic prostaglandin D2 synthase in the control of delayed type hypersensitivity, Proc. Natl. Acad. Sci. USA 103 (2006) 5179–5184.
[43] K. Kabashima, D. Sakata, M. Nagamachi, Y. Miyachi, K. Inaba, S. Narumiya, Prostaglandin E_2-EP_4 signalling initiates skin immune responses by promoting migration and maturation of Langerhans cells, Nat. Med. 9 (2003) 744–749.
[44] G. Taguchi, Experimental Designs, Maruzen, Tokyo, 1962.
[45] L.J.II. Roberts, B.J. Sweetman, R.A. Lewis, K.F. Austen, J.A. Oates, Increased production of prostaglandin D_2 in patients with systemic mastocytosis, N. Engl. J. Med. 303 (1980) 1400–1404.
[46] J.A. Boyce, Eicosanoid mediators of mast cells: receptors, regulation of synthesis, and pathobiologic implications, Chem. Immunol. Allergy 87 (2005) 59–79.
[47] L.J.II. Roberts, R.A. Lewis, J.A. Oates, K.F. Austen, Prostaglandin thromboxane, and 12-hydroxy-5,8,10,14-eicosatetraenoic acid production by ionophore-stimulated rat serosal mast cells, Biochim. Biophys. Acta 575 (1979) 185–192.

doi: 10.1111/j.1365-3083.2007.02020.x

A Genetic Locus Controlling Aging-sensitive Regression of B Lymphopoiesis in an Autoimmune-prone MRL/lpr Strain of Mice

K. Nakatani*, W.-M. Qu†, M.-C. Zhang‡, H. Fujii†, H. Furukawa‡, T. Miyazaki†, M. Iwano*, Y. Saito*, M. Nose† & M. Ono‡

*First Department of Internal Medicine, Nara Medical University, Kashihara, Japan; †Department of Pathology, Ehime University School of Medicine, Toon, Japan; and ‡Department of Pathology, Tohoku University Graduate School of Medicine, Sendai, Japan

Received 20 June 2007; Accepted in revised form 14 August 2007

Correspondence to: M. Ono, Department of Pathology, Tohoku University Graduate School of Medicine, 2-1 Seiryo, Aoba-ku, Sendai, Miyagi 980-8575, Japan. E-mail: onomasao@mail.tains.tohoku.ac.jp

Abstract

Aging readily affects immune system under the influence of environmental and/or intrinsic factors while accelerating the development of various immune disorders including autoimmune diseases. Little is known about molecular and cellular mechanisms connecting between immune senescence and development of autoimmune diseases. Here, we first show strain-specific and aging-sensitive onset of B-cell abnormality in a lupus-prone MRL/Mp.Fas^{lpr} (MRL/lpr) strain of mice. This abnormality was characterized by the regression of B lymphopoiesis in the bone marrow of this strain. We next examined the association between the B-cell regression and onset of autoimmune diseases in aged (MRL/lpr × C3H/He.Fas^{lpr}) F_2 mice, in which pathologic phenotypes, such as glomerulonephritis, vasculitis, sialoadenitis and arthritis, variously developed. We also searched whole genome to identify genetic loci linked to the B-cell regression by using the same F_2 mice. The B-cell regression manifested in the spleen of F_2 mice was retrospectively evaluated by reverse transcriptase-based PCR quantification. The results demonstrated that the onset of autoimmune diseases in the F_2 mice was not associated with the aging-sensitive B-cell regression. The genetic study identified a significant locus responsible for the B-cell regression in the vicinity of *D5Mit233* (29 cM). This is first evidence for the presence of a genetic locus that affects B lymphopoiesis in an aging-sensitive manner.

Introduction

Homeostasis of immune system is essential for the integrity of our life. However, a state of immune homeostasis is thought to be changeable in response to intrinsic and environmental conditions. For example, aging as an intrinsic condition results in the regression of immune functions; a hygiene condition that influences an immune condition, i.e. a case of type 2 helper T-cell (Th2)-deviation presumably established under a modern hygiene condition and associated with human allergic disorders. It is a general understanding that a change in immune homeostasis has an impact on pathogenic mechanisms underlying various immune and infectious diseases. Aging is thought to be an important intrinsic factor for changing immune homeostasis, but little is known about an aging-sensitive homeostatic and pathogenic immune condition.

An animal experiment usually has the advantage of invariant genetic and environmental condition and provides an opportunity for longitudinal observation. An inbred strain of mice MRL/Mp.Fas^{lpr} (MRL/lpr) represents a model for human autoimmune diseases, which spontaneously develops lupus-like glomerulonephritis, systemic vasculitis, arthritis and sialadenitis [1–4]. An MRL/lpr strain carries a loss-of-function mutation of Fas gene (*lpr*) which encodes an apoptosis receptor on lymphocytes [5]. The *lpr* mutation is necessary for the onset of autoimmune diseases in MRL/lpr; however, the other *lpr*-congenic strains, including C3H/He.Fas^{lpr} (C3H/lpr), C57BL/6.Fas^{lpr} and AKR.Fas^{lpr}, barely develop autoimmune diseases [6–9]. The strain difference in the lpr constraint also influences the longevity of mice. An average age of death was estimated to be 17 weeks for female MRL/lpr, 22 weeks for male MRL/lpr and between 42 and 52 weeks for females on the C57BL/6J or C3H/HeJ

background (Mouse Genome Informatics, http://www.informatics.jax.org/menus/strain_menu.shtml). These facts indicate that the *lpr* mutation is not sufficient for the onset of autoimmune diseases, and that MRL/Mp-specific genetic conditions are prerequisite to the disease onset.

A number of studies have shown that Fas is essential for the prevention of autoreactive B-cell expansion [10–12]. In these studies, transgenic mouse models expressing autoantibody-encoding genes on B cells were studied when compared between Fas-deficient and Fas-sufficient strains. There is limited information on genetic background-specific autoimmune phenotype of B cells. To address this issue, we have used a non-autoimmune-prone C3H/lpr strain as well as a Fas-sufficient MRL/Mp (MRL/+) strain as reference strains for MRL/lpr. The combined use of these three strains enables us to evaluate effects of MRL/Mp-specific genetic factor and *lpr* on the onset of various autoimmune traits. Thereby, we have been attempting to identify strain-specific immune phenotypes and genetic polymorphisms associated with autoimmune diseases in MRL/lpr.

An autoimmune-prone strain of mice – BXSB – exhibits regression of B lymphopoiesis with aging [13]. This study proposed an aetiological link between this B-cell abnormality and autoimmune phenotypes in this strain. B cells expressing a single-antigen specificity to hen egg lysozyme (HEL) show spontaneous hyperactivity in the absence of self-antigen in MRL/lpr background [14]. Notably, this stain of mice was not only shown to have low total B-cell numbers but also an expansion of the marginal zone B-cell population. The proposed link remains to be shown in autoimmune strains of mice including MRL/lpr.

In the initial phase of the present study, we demonstrated a aging-dependent, significant decrease in the expression of FcγRIIb1 and CD22 in the spleen of MRL/lpr. FcγRIIb1 and CD22 are inhibitory receptors which physiologically regulate B-cell functions. A defect in either function of these receptors is known to entail autoimmune diseases in mice; therefore, their inhibitory functions are essential for the prevention of autoimmunity in B cells [15, 16]. Moreover, the genetic polymorphisms of these receptor genes have been suggested to be associated with autoimmune diseases in humans and mice [17–19]. The phenotype regarding FcγRIIb1 or CD22 is considered as a critical, causal impact on autoimmune diseases.

Genetic studies using autoimmune-prone strains of mice have revealed that the onset of most autoimmune traits is controlled by complex loci. Our previous studies using (MRL/lpr × C3H/lpr) (MC) F_2 mice identified differential sets of susceptibility loci controlling organ/tissue specificity of autoimmune disease [8], suggesting that background genes other than *lpr* determine tissue specificity of autoimmune disease. Here, we took advantage of accumulated data on the MCF_2 mice to evaluate an association between the B-cell regression and tissue-specific onset of autoimmune disease. Furthermore, we attempted to identify a responsible locus for the B-cell regression in the spleen by using the genome-wide microsatellite data of these mice. This study provides first evidence for the presence of genetic predisposition controlling B lymphopoiesis in an aging-sensitive manner.

Materials and methods

Mice. MRL/lpr and MRL/+ were purchased from Charles River Japan (Tokyo, Japan). C3H/lpr was purchased from The Jackson Laboratory (Bar Harbor, ME, USA). These mice were bred under specific pathogen-free conditions in the Integrated Center of Science, Ehime University, or the Animal Research Institute of Tohoku University Graduate School of Medicine. MCF_1 and MCF_2 mice were generated from female MRL/lpr and male C3H/lpr. In all animal experiments in this study, we observed the Tohoku University guideline or the Ehime University guideline for animal experimentation.

Flow cytometry. Spleen cells (10^6) were stained with the recommended dilution of fluorescence- or biotin-conjugated antibody in PBS containing 1% BSA on ice. All antibodies used in this study were purchased (BD PharMingen, San Diego, CA, USA). Streptavidin-conjugated allophycocyanin was used with a biotinylated antibody. We analysed small lymphocytic cells on the CellQuest software (Becton Dickinson, San Jose, CA, USA).

Reverse transcriptase-based PCR. Total RNA was isolated from spleen with ISOGEN (Nippon Gene, Tokyo, Japan). A first-strand cDNA was synthesized using random primer (Invitrogen, Carlsbad, CA, USA). Serially diluted cDNA products were subjected to reverse transcriptase-based PCR (RT-PCR) analyses. The transcripts were amplified by the following primers and conditions: FcγRIIb1/b2, AAGTCTAGGAAGGACACTGC and ATCCTGGCCTTTCTGGCTTGC, 28 cycles of 94 °C for 30 s, 55 °C for 30 s and 72 °C for 30 s; FcγRIIb1, AAGTCTAGGAAGGACACTGC and CCTCTGGAAGGGTTTCTCCCA, 20 cycles of 94 °C for 30 s, 55 °C for 30 s and 72 °C for 30 s; CD22, AAACTCCACTACCCAAGG and AGGTGATCTTAGAATCTTCC, 18 cycles of 94 °C for 30 s, 54 °C for 30 s and 72 °C for 30 s; CD19, AATCAGAGTCTAATCAACCAAG and GCCACCAGAGAAACCATACAGAAG by 18 cycles of 94 °C for 30 s, 55 °C for 30 s and 72 °C for 30 s; FcRγ, ATGATCTCAGCCGTGATCTTG and CTACTGGGGTGGTTTCTCATGCT, 22 cycles of 94 °C for 30 s, 55 °C for 30 s and 72 °C for 30 s; HPRT, GCTGGTGAAAAGGACCTCT and CACAGGACTAGAACACCTGC by 25 cycles of 94 °C for 30 s, 55 °C for 30 s and 72 °C for 30 s. PCR products were fractionated by electrophoresis in 2% agarose gel and were visualized after ethidium bromide staining.

A quantitative analysis was performed by real-time PCR system using the ABI Prism 7700 Sequence Detection System (Perkin-Elmer Applied Biosystems, Foster City, CA, USA). The FcγRIIb1 TaqMan™ probe (Perkin-Elmer Applied Biosystems) was CTATCTCAAGAAAAAGCAGGTTCCAGCTCTCCC. The forward and reverse primers for FcγRIIb1 amplification were GCAGCCATTGTTATTATCCTAGTATCC and CCTCTGGAAGGGTTTCTCCCA respectively. The CD22 TaqMan™ probe was TCCTCGGAGGCTGCGTGTGTCC. The forward and reverse primers for CD22 amplification were ATCGGAGAGACCTTGTCACAGG and ACTGTGAGATGGGCGGATTG respectively. The 18S rRNA TaqMan™ probe set was obtained from TaqMan™ Rodent 18S rRNA Control Reagents (Perkin-Elmer Applied Biosystems). The expression of FcγRIIb1, CD22 and 18S rRNA were quantified in separate tubes. We confirmed no amplification with the sample prepared in the absence of reverse transcriptase, indicating that a false signal originated from genomic DNA was negligible.

Histopathological examinations. All mice were killed under ether anesthesia at 16–20 weeks of age. We used histopathological grades determined previously for glomerulonephritis [20], arthritis [21–23], vasculitis [24, 25] and sialadenitis [26].

Microsattelite analysis and statistics. Genome-wide genotyping data of the MCF_2 mice determined in our previous study were used again in this study [26]. A hundred and six microsatellite markers cover whole autosomes with 12 cM apart with a maximum distance between any two markers of 37 cM. The positions of microsatellite loci were based on information from the Mouse Genome Database (MGD), The Jackson Laboratory (http://www.informatics.jax.org/menus/strain_menu.shtml). Association between genotype and expression index of FcγRIIb1 or CD22 was evaluated by an ANOVA. Significant and suggestive association was estimated based on a value of $P < 0.000052$ and $P < 0.0016$, respectively, as recommended by Lander and Kruglyak [27]. Quantitative trait locus (QTL) on chromosome 5 was determined with the data from 198 MCF_2 mice and the 11 microsatellite markers as indicated in Fig. 4. The mRNA expression levels of FcγRIIb1 and CD22 were $\log_{10}$ transformed. Logarithmic odds (LOD) scores were calculated by the interval mapping and the composite interval mapping methods in the Windows QTL Cartographer (Ver 2.5) software [28]. We adopted Model 6 with forward and backward regression methods for composite interval mapping. The number of control markers, the window size and the walk speed were set at 5, 10 cM and 2 cM respectively. A significant level was determined with the permutation test (1000 times) developed by Churchill and Doerge [29]. Difference of mean values of two groups was evaluated by the two-tailed multiple *t*-test with Bonferroni correction following an ANOVA.

Results

Aging-sensitive decrease in B-cell in the spleen of MRL/lpr mice

Comparing immune phenotypes between MRL/lpr and C3H/lpr, we eventually identified a marked change in the expression pattern of FcγRIIb1 and FcγRIIb2 in the spleen of 20-week-old MRL/lpr mice (Fig. 1A). The decrease was not observed in 8-week-old MRL/lpr mice. *FcγRIIB* gene is known to generate two alternative splicing products, FcγRIIb1 and FcγRIIb2. In spleen, FcγRIIb1 is expressed in B cells, while FcγRIIb2 is expressed in monocyte/macrophage and myeloid lineaged cells [30, 31]. Fig. 1A indicated a drastic conversion of FcγRIIb1/b2 ratio in the spleen of aged MRL/lpr mice, suggestive of a decrease in FcγRIIb1 expression, an increase in FcγRIIb2 expression or both. To address this concern, we examined relative protein amounts of FcγRIIb1 and FcγRIIb2 in the spleen by means of immunoprecipitation followed by Western blotting with FcγRIIb1/b2-specific antiserum. No evidence was obtained for relative increase in FcγRIIb2 protein expression (Fig. 1B), indicating that a decrease in FcγRIIb1 expression is a major event in the spleen of aged MRL/lpr mice.

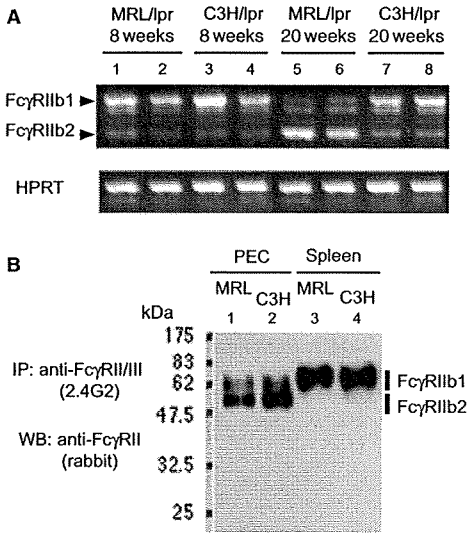

Figure 1 Expression of FcγRIIB isoforms (*FcγRIIb1 and FcγRIIb2*) in autoimmune-prone MRL/lpr and non-autoimmune-prone C3H/lpr mice. (A) RT-PCR assay showing aging-sensitive relative decrease in FcγRIIb1 expression in the spleen of aged (20-week-old) MRL/lpr mice. RT-PCR products obtained from two individual spleens were shown by ethidium bromide staining on an agarose gel. The comparable signal intensities of HPRT indicate equal loads of cDNA for all lanes. (B) Western blot analysis showing protein expression of FcγRIIB isoforms in the spleen and thioglycolate-induced peritoneal cells (PEC) in aged mice. MRL, aged MRL/lpr; C3H, aged C3H/lpr; IP, immunoprecipitation; WB, Western blot. Molecular weights (kDa) are indicated.

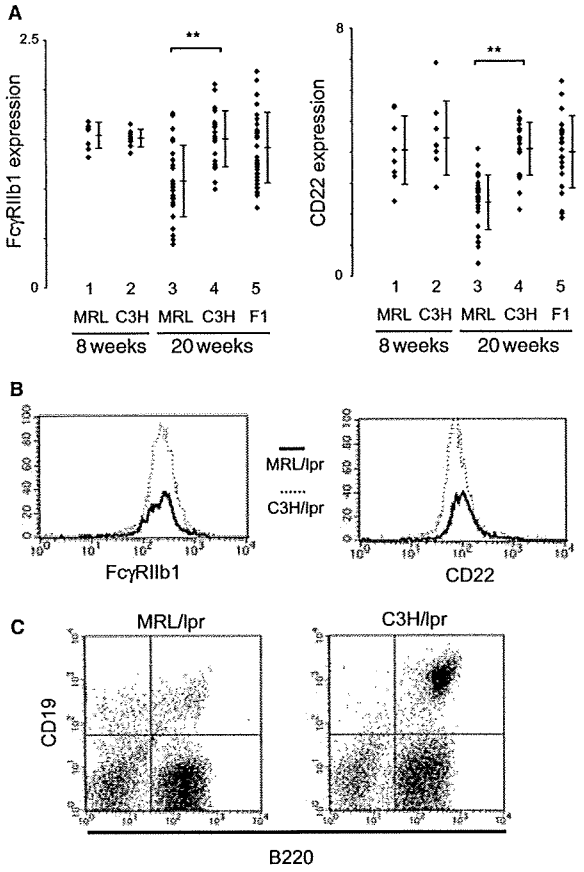

Figure 2 B-cell-related phenotypes in spleen. (A) RT-PCR quantification using the TaqMan™ probe showing significant decrease in FcγRIIb1 and CD22 expression in the spleen of an indicated strain of mice. Each bar represents the mean ± SD in each group. The difference of mean values of two groups was evaluated by the two-tailed multiple *t*-test with Bonferroni correction following one-way ANOVA. $^{**}P < 0.01$. (B) Flow cytometric analysis for B cells in the spleen of aged mice. B cells were gated as CD19-positive cells. The histogram showing a cell-surface expression level of FcγRIIb1 and CD22 protein. Three assays reproduced the same results. (C) Flow cytometric analysis using antibodies to CD45R (*B220*) and CD19 for the spleen cells of aged mice. Double-positive fraction includes B cells. CD45R (*B220*) single-positive cells are known to be *lpr*-T cells which uniquely appear in the Fas-deficient condition. This is a representative result summarized in Table 1 ($n = 4$).

Aging-sensitive and strain-dependent decrease in FcγRIIb1 expression in the spleen was confirmed for a large number of spleen samples by RT-PCR with FcγRIIb1-specific PCR primers (Fig. 2A). Another B-cell-specific molecule, CD22, represented an expression pattern similar to FcγRIIb1 (Fig. 2A). A flow cytometric analysis revealed comparable expression of FcγRIIb1 and CD22 protein on a single B cell (Fig. 2B). Importantly, spleen cell counts and a flow cytometric analysis with B-cell-specific markers, CD45R (denoted as B220 in the present figures) and CD19, confirmed a relative and absolute decrease in B-cell numbers in the spleen of aged MRL/lpr mice (Table 1, Fig. 2C). This tendency was observed in aged *Fas*-sufficient MRL/+ mice (Table 1).

Aging-sensitive decrease in B lymphopoiesis in MRL/lpr mice

A flow cytometric analysis using lineage markers for B-cell development revealed a remarkable decrease in B-cell precursors ($B220^+$ IgM^-), immature B cells ($B220^+$ IgM^+) and mature B cells ($B220^{high+}$ IgM^+) in the bone marrow of aged MRL/lpr (Table 1, Fig. 3A). This tendency was observed in aged MRL/+ mice (Table 1). RT-PCR assays consistently revealed a lower expression of B-cell-related transcripts, such as FcγRIIb1, CD22 and CD19, in the bone marrow of aged MRL/lpr mice, supporting the decrease in B lineage cells. On the other hand, Fc receptor gamma chain (FcRγ) was comparably detected for both strains (Fig. 3B). Overall findings indicate that the regression of B lymphopoiesis occurs in an aging-sensitive and MRL background-dependent fashion.

Association between the B-cell regression and onset of autoimmune diseases

We examined the association between the expression of B-cell-related transcripts, FcγRIIb1 and CD22, in the spleen and onset of autoimmune diseases in the MCF_2 mice. Statistically significant association was not observed with glomerulonephritis, renal vasculitis, sialadenitis or arthritis (Table 2).

A responsible locus for the B-cell regression

Using the genotype data of the MCF_2 mice determined previously [20, 26], we searched whole genome for genetic loci responsible for the B-cell regression in the MCF_2 mice. An MRL/lpr allele at *D5Mit233* (29 cM) was shown to be associated with a decrease in FcγRIIb1 expression in a recessive inheritance mode (Table 3). There was a clear tendency for an association between this locus genotype and CD22 expression in the same fashion; however, it was not statistically supported (Table 3). The interval and composite interval mapping of a QTL analysis demonstrated a single LOD peak at 26 cM and 24 cM for FcγRIIb1 and CD22 traits respectively (Fig. 4). Threshold levels of LOD with statistical significance were estimated to be 3.24 ($\alpha = 0.01$) and 2.26 ($\alpha = 0.05$) for FcγRIIb1 loci and 3.01 ($\alpha = 0.01$) and 2.25 ($\alpha = 0.05$) for CD22 loci by the permutation test.

Discussion

The present study provided first evidence for aging-dependent regression of B lymphopoiesis in an

Table 1 The number or fraction of B lineage cells in the spleen and bone marrow of aged MRL and C3H mice.

	Genotype	Unit	Strain of mice MRL	C3H	Statistics[a]
Spleen					
Total cell counts	*lpr/lpr*	$\times 10^6$	278 (63.1)	260 (26.9)	
	+/+	$\times 10^6$	37.5 (8.70)	45.3 (8.54)	
B cells ($B220^+$ $CD19^+$)	*lpr/lpr*	$\times 10^6$	20.9 (15.9)	87.7 (18.4)	**
	+/+	$\times 10^6$	8.43 (1.54)	14.9 (1.96)	**
Bone marrow					
B precursors (IgM^-B220^+)	*lpr/lpr*	%	10.9 (2.82)	26.6 (3.54)	**
	+/+	%	6.25 (1.17)	14.4 (2.16)	**
Immature B (IgM^+B220^+)	*lpr/lpr*	%	3.48 (1.23)	5.75 (0.57)	*
	+/+	%	2.60 (0.67)	4.43 (0.53)	**
Mature B (IgM^+B220^{++})	*lpr/lpr*	%	1.55 (0.87)	6.65 (1.30)	**
	+/+	%	4.98 (1.58)	8.08 (1.30)	*

[a]Two-tailed *t*-test: $**P < 0.01$; $*P < 0.05$.
Each value represents the mean (SD) of four mice.

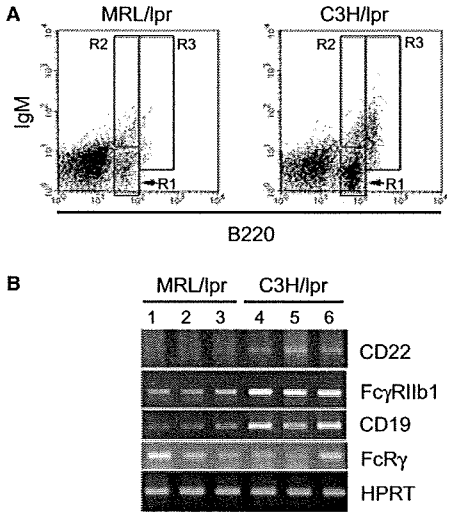

Figure 3 B-cell-related phenotypes in bone marrow. (A) Flow cytometric analysis using antibodies to CD45R (*B220*) and IgM showing the development of B cells in the bone marrow cells of aged mice. Indicated boxes in the dot-gram include pro- and pre-B cells (*R1*), immature B cells (*R2*) and mature B cells (*R3*). This is a representative result summarized in Table 1 ($n = 4$). (B) RT-PCR assay showing relative decrease in B-cell-related transcripts (*CD22*, *FcγRIIb1* and *CD19*) in the bone marrow of aged (20-week-old) MRL/lpr mice. RT-PCR products obtained from three individual spleens were shown by ethidium bromide staining on agarose gels. The comparable signal intensities of HPRT indicate equal loads of cDNA for all lanes.

MRL/lpr lupus strain and genetic regulation of this phenotype. It is of particular note that this phenotype depends on strain-specific genetic background but not on the *lpr* mutation. The significance of genetic background has been emphasized in the lpr-dependent autoimmunity. It has been explored how the genetic background alters immune phenotypes toward autoimmune diseases in an MRL/lpr strain. If such phenotype was found, it would be accounted as a cellular target for autoimmune therapy. In the initial phase of this study, we found a remarkable, strain-specific, *lpr*-independent decrease in peripheral B-cell number in MRL/lpr mice. These findings facilitated us to investigate the correlation between the B-cell regression and autoimmune onset. The MCF_2 mice, which were previously generated to identify QTL of autoimmune diseases, provided us with an opportunity for the evaluation of the correlation. The results rather indicate that the B-cell regression in MRL/lpr mice is not a cause of autoimmune disease. This conclusion is also supported by the genetic findings that the present locus located near *D5Mit233* does not overlap with any of autoimmune loci previously identified in associations with glomerulonephritis [20], arthritis [21–23], vasculitis [24, 25] and sialadenitis [26]. We failed to show the significant association of this phenotype with the onset of glomerulonephritis, ranal arthritis, vasculitis and sialadenitis. Other autoimmune phenotypes such as pancreatitis and a series of autoantibody production should be investigated. It is also an interesting question whether the B-cell regression of interest influences susceptibility to vaccinated antigen or infection.

Hypergamma globulinemia is generally characteristic of autoimmune disease. MRL/lpr mice readily exhibit this trait with aging and disease onset. The decline of B-cell numbers in the spleen and bone marrow with aging in MRL/lpr seems to conflict with prominent hypergamma globulinemia in this strain. Similar to the MRL/lpr case, a remarkable decrease in B lymphopoiesis with aging was demonstrated in another autoimmune-prone BXSB strain of mice [13]. Another study has shown that B cells expressing single-antigen specificity to HEL represent spontaneous hyperactivity in the absence of self-antigen in MRL/lpr background. Notably, this stain of mice was not only shown to have low total B-cell

Table 2 Association of FcγRIIbl or CD22 expression with the autoimmune trait manifested in MCF_2 mice.

	FcγRIIbl			CD22		
	Onset of disease[a]			Onset of disease[a]		
	+	−	P^b	+	−	P^b
Glomerulonephritis	0.96 (0.42)	0.97 (0.39)	0.883	2.49 (0.92)	2.71 (1.22)	0.213
Renal vasculitis	0.98 (0.39)	0.97 (0.40)	0.905	2.68 (1.14)	2.66 (1.16)	0.935
Arthritis	1.00 (0.40)	0.97 (0.40)	0.696	2.66 (1.17)	2.66 (1.16)	0.990
Sialadenitis	0.98 (0.37)	0.96 (0.41)	0.825	2.63 (1.12)	2.67 (1.22)	0.769

[a]Onset of each disease was defined in the previous reports (see *Materials and methods*). +, diseased; −, not affected.
[b]Two-tailed *t*-test.
Each value represents the mean (SD) of FcγRIIbl or CD22 expression index.

Table 3 Association of FcγRIIbl and CD22 expression with microsatellite genotypes on chromosome 5.

		Genotype			
Marker	cM	MM^a	MC^a	cc^a	P^b
FcγRIIbl expression					
D5Mit145	0	0.86 (0.34)	0.98 (0.41)	1.07 (0.40)	0.025
D5Mit74	11	0.84 (0.34)	1.00 (0.42)	1.05 (0.38)	0.0037
D5Mit149	19	0.80 (0.34)	1.02 (0.42)	1.03 (0.37)	0.00085[c]
D5Mit233	29	0.80 (0.28)	1.04 (0.46)	1.02 (0.33)	0.00015[c]
D5Mit134	41	0.83 (0.28)	1.01 (0.46)	1.05 (0.33)	0.0025
D5Mit115	56	0.86 (0.30)	1.01 (0.47)	1.01 (0.31)	0.0270
CD22 expression					
D5Mit145	0	2.31 (0.90)	2.68 (1.13)	2.95 (1.35)	0.017
D5Mit74	11	2.30 (0.97)	2.73 (1.12)	2.92 (1.32)	0.0076
D5Mit149	19	2.23 (0.97)	2.77 (1.12)	2.84 (1.27)	0.0046
D5Mit233	29	2.25 (1.04)	2.81 (1.10)	2.80 (1.28)	0.0053
D5Mit134	41	2.40 (1.12)	2.64 (1.10)	2.93 (1.25)	0.054
D5Mit115	56	2.41 (1.10)	2.69 (1.13)	2.86 (1.24)	0.092

[a]*MM*, *MC* and *CC* represent the genotypes at indicated marker positions: MRL/MRL homozygote, MRL/C3H heterozygote and C3H/C3H homozygote respectively.
[b]One-way layout ANOVA.
[c]Suggestive linkage.
Each value represents the mean (SD) in each genotype group.

numbers but also an expansion of the marginal zone B-cell population. These findings may lead to a new insight revealing general correlation between B-cell regression and autoimmune onset.

Here, we demonstrated the regression of B lymphopoiesis in not only autoimmune MRL/lpr mice but also non-autoimmune MRL/+ mice. This finding suggests that the B-cell regression is not an effect of autoimmunity. Functional B cells are established after undergoing multiple differentiation stages in bone marrow and peripheral lymphoid tissues. Aging has been shown to spontaneously, readily impair B lymphopoiesis [32–34]. A molecular mechanism of the impact of aging on B lymphopoiesis remains unclear. The genetic information obtained from this study provides a clue to clarify this issue.

The locus identified in this study includes candidate genes that function with immunological importance. This locus is syntenic of human chromosome interval between 4p14 and 4p16.3. Considering gene functions for B-cell activation and differentiation, we presently evaluate *Bst1* (bone marrow stromal cell antigen 1, 25 cM) and *Cd38* (CD38, 28 cM) as the positional candidates. The two genes encode a similar type of cell surface receptors belonging to the super family of ADP-ribosyl cyclase. *Bst1* product is present on bone marrow stromal cells which regulate B lymphopoiesis [35]. *Cd38* product is present on B lineage cells and serve as a receptor which mediates the signal for the suppression of B lymphopoiesis [36, 37] and the modulation of B-cell functions [38, 39]. Polymorphic nature of these molecules is of primary interest as concerning the B-cell regression manifested in MRL/lpr mice.

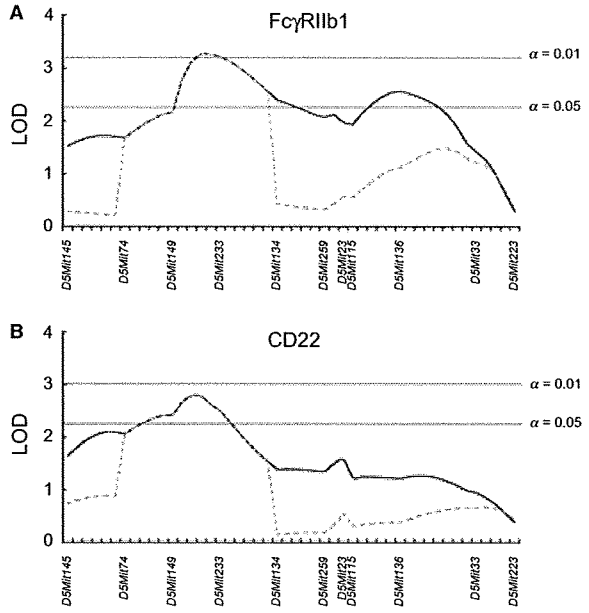

Figure 4 Plots of the logarithmic odds (LOD) scores of QTL on chromosome 5 for the expression of FcγRIIb1 (A) and CD22 (B) transcript in the spleen of MCF_2 mice. Solid and broken lines indicate the results from interval mapping and composite interval mapping analysis respectively. We adopted the composite interval mapping method of Model 6 in the Windows QTL Cartographer (V2.5) software. The control marker number and window size were 5 and 10 cM respectively. Horizontal lines indicate the threshold levels of significant LOD determined by the permutation test installed in this programme (1000 times permutations, a = 0.01 for upper line, a = 0.05 for lower line). Genetic positions of MIT markers are indicated on the horizontal axis.

Acknowledgment

The authors thank Mrs H. Ohura for technical assistances, the members of the Integrated Center for Sciences (INCS), Ehime University for animal breeding, and Mrs N. Fujisawa for secretarial assistance. This study was supported by Grants-in-Aid for Scientific Research from the Ministry of Education, Science, Sports, and Culture of Japan to MO (19390108 and 19659096).

References

1 Andrews BS, Eisenberg RA, Theofilopoulos AN *et al.* Spontaneous murine lupus-like syndromes. Clinical and immunopathological manifestations in several strains. *J Exp Med* 1978;148:1198–215.

2 Morse HC III, Davidson WF, Yetter RA, Murphy ED, Roths JB, Coffman RL. Abnormalities induced by the mutant gene Ipr: expansion of a unique lymphocyte subset. *J Immunol* 1982;129:2612–5.

3 Jonsson R, Tarkowski A, Backman K, Holmdahl R, Klareskog L. Sialadenitis in the MRL-l mouse: morphological and immunohistochemical characterization of resident and infiltrating cells. *Immunology* 1987;60:611–6.

4 Hang L, Theofilopoulos AN, Dixon FJ. A spontaneous rheumatoid arthritis-like disease in MRL/l mice. *J Exp Med* 1982;155:1690–701.

5 Watanabe-Fukunaga R, Brannan CI, Copeland NG, Jenkins NA, Nagata S. Lymphoproliferation disorder in mice explained by defects in Fas antigen that mediates apoptosis. *Nature* 1992;356:314–7.

6 Izui S, Kelley VE, Masuda K, Yoshida H, Roths JB, Murphy ED. Induction of various autoantibodies by mutant gene lpr in several strains of mice. *J Immunol* 1984;133:227–33.

7 Kelley VE, Roths JB. Interaction of mutant lpr gene with background strain influences renal disease. *Clin Immunol Immunopathol* 1985;37:220–9.

8 Nose M, Nishihara M, Fujii H. Genetic basis of the complex pathological manifestations of collagen disease: lessons from MRL/lpr and related mouse models. *Int Rev Immunol* 2000;19:473–98.

9 Zhang MC, Misu N, Furukawa H *et al.* An epistatic effect of the female specific loci on the development of autoimmune vasculitis and antinuclear autoantibody in murine lupus. *Ann Rheum Dis* 2006;65:495–500.

10 Roark JH, Kuntz CL, Nguyen KA, Mandik L, Cattermole M, Erikson J. B cell selection and allelic exclusion of an anti-DNA Ig transgene in MRL-lpr/lpr mice. *J Immunol* 1995;154:4444–55.

11 Kench JA, Russell DM, Nemazee D. Efficient peripheral clonal elimination of B lymphocytes in MRL/lpr mice bearing autoantibody transgenes. *J Exp Med* 1998;188:909–17.

12 Mandik-Nayak L, Seo S, Eaton-Bassiri A, Allman D, Hardy RR, Erikson J. Functional consequences of the developmental arrest and follicular exclusion of anti-double-stranded DNA B cells. *J Immunol* 2000;164:1161–8.

13 Jyonouchi H, Kincade PW, Good RA. Age-dependent changes in B lymphocyte lineage cell populations of autoimmune-prone BXSB mice. *J Immunol* 1985;134:858–64.

14 Nijnik A, Ferry H, Lewis G *et al.* Spontaneous B cell hyperactivity in autoimmune-prone MRL mice. *Int Immunol* 2006;18:1127–37.

15 Bolland S, Ravetch JV. Spontaneous autoimmune disease in Fc(gamma)RIIB-deficient mice results from strain-specific epistasis. *Immunity* 2000;13:277–85.

16 Cornall RJ, Cyster JG, Hibbs ML *et al.* Polygenic autoimmune traits: Lyn, CD22, and SHP-1 are limiting elements of a biochemical pathway regulating BCR signaling and selection. *Immunity* 1998;8:497–508.

17 Jiang Y, Hirose S, Abe M *et al.* Polymorphisms in IgG Fc receptor IIB regulatory regions associated with autoimmune susceptibility. *Immunogenetics* 2000;51:429–35.

18 Mary C, Laporte C, Parzy D *et al.* Dysregulated expression of the Cd22 gene as a result of a short interspersed nucleotide element insertion in Cd22a lupus-prone mice. *J Immunol* 2000;165:2987–96.

19 Kyogoku C, Dijstelbloem HM, Tsuchiya N *et al.* Fcgamma receptor gene polymorphisms in Japanese patients with systemic lupus erythematosus: contribution of FCGR2B to genetic susceptibility. *Arthritis Rheum* 2002;46:1242–54.

20 Miyazaki T, Ono M, Qu WM *et al.* Implication of allelic polymorphism of osteopontin in the development of lupus nephritis in MRL/lpr mice. *Eur J Immunol* 2005;35:1510–20.

21 Kamogawa J, Terada M, Mizuki S *et al.* Arthritis in MRL/lpr mice is under the control of multiple gene loci with an allelic combination derived from the original inbred strains. *Arthritis Rheum* 2002;46:1067–74.

22 Mori S, Zhang MC, Tanda N *et al.* Genetic characterisation of spontaneous ankylosing arthropathy with unique inheritance from Fas-deficient strains of mice. *Ann Rheum Dis* 2006;65:1273–8.

23 Zhang MC, Mori S, Date F, Furukawa H, Ono M. A non-major histocompatibility locus determines tissue specificity in the pathogenic process underlying synovial proliferation in a mouse arthropathy model. *Ann Rheum Dis* 2007;66:242–5.

24 Qu WM, Miyazaki T, Terada M *et al.* Genetic dissection of vasculitis in MRL/lpr lupus mice: a novel susceptibility locus involving the CD72c allele. *Eur J Immunol* 2000;30:2027–37.

25 Yamada A, Miyazaki T, Lu LM *et al.* Genetic basis of tissue specificity of vasculitis in MRL/lpr mice. *Arthritis Rheum* 2003;48:1445–51.
26 Nishihara M, Terada M, Kamogawa J *et al.* Genetic basis of autoimmune sialadenitis in MRL/lpr lupus-prone mice: additive and hierarchical properties of polygenic inheritance. *Arthritis Rheum* 1999;42:2616–23.
27 Lander E, Kruglyak L. Genetic dissection of complex traits: guidelines for interpreting and reporting linkage results. *Nat Genet* 1995;11:241–7.
28 Zeng ZB. Precision mapping of quantitative trait loci. *Genetics* 1994;136:1457–68.
29 Churchill GA, Doerge RW. Empirical threshold values for quantitative trait mapping. *Genetics* 1994;138:963–71.
30 Ravetch JV, Luster AD, Weinshank R *et al.* Structural heterogeneity and functional domains of murine immunoglobulin G Fc receptors. *Science* 1986;234:718–25.
31 Amigorena S, Bonnerot C, Choquet D, Fridman WH, Teillaud JL. Fc gamma RII expression in resting and activated B lymphocytes. *Eur J Immunol* 1989;19:1379–85.
32 Stephan RP, Sanders VM, Witte PL. Stage-specific alterations in murine B lymphopoiesis with age. *Int Immunol* 1996;8:509–18.
33 Stephan RP, Lill-Elghanian DA, Witte PL. Development of B cells in aged mice: decline in the ability of pro-B cells to respond to IL-7 but not to other growth factors. *J Immunol* 1997; 158:1598–609.
34 Stephan RP, Reilly CR, Witte PL. Impaired ability of bone marrow stromal cells to support B-lymphopoiesis with age. *Blood* 1998;91:75–88.
35 Kaisho T, Ishikawa J, Oritani K *et al.* BST-1, a surface molecule of bone marrow stromal cell lines that facilitates pre-B-cell growth. *Proc Natl Acad Sci USA* 1994;91:5325–9.
36 Kumagai M, Coustan-Smith E, Murray DJ *et al.* Ligation of CD38 suppresses human B lymphopoiesis. *J Exp Med* 1995;181:1101–10.
37 Kitanaka A, Ito C, Nishigaki H, Campana D. CD38-mediated growth suppression of B-cell progenitors requires activation of phosphatidylinositol 3-kinase and involves its association with the protein product of the c-cbl proto-oncogene. *Blood* 1996;88: 590–8.
38 Yamashita Y, Miyake K, Kikuchi Y *et al.* A monoclonal antibody against a murine CD38 homologue delivers a signal to B cells for prolongation of survival and protection against apoptosis *in vitro*: unresponsiveness of X-linked immunodeficient B cells. *Immunology* 1995;85:248–55.
39 Funaro A, Morra M, Calosso L, Zini MG, Ausiello CM, Malavasi F. Role of the human CD38 molecule in B cell activation and proliferation. *Tissue Antigens* 1997;49:7–15.

Ultrasound in Med. & Biol., Vol. 34, No. 3, pp. 425–434, 2008

0301-5629/08/$–see front matter

ELSEVIER

doi:10.1016/j.ultrasmedbio.2007.09.004

● *Original Contribution*

HERPES SIMPLEX VIRUS THYMIDINE KINASE-MEDIATED SUICIDE GENE THERAPY USING NANO/MICROBUBBLES AND ULTRASOUND

ATSUKO AOI,*† YUKIKO WATANABE,* SHIRO MORI,‡ MASAHIKO TAKAHASHI,† GEORGES VASSAUX,§‖ and TETSUYA KODAMA*

*Biomedical Engineering Research Organization, Tohoku University, †Graduate School of Dentistry, Tohoku University, ‡Tohoku University Hospital, Sendai, Japan; and §INSERM CIC-004, ‖Institut des maladies de l'Appareil Digestif, CHU Hotel Dieu, Nantes, France

(*Received* 12 *January* 2007, *revised* 25 *June* 2007, *in final form* 5 *September* 2007)

Abstract—A physical method using ultrasound (US) and nano/microbubbles (NBs) can deliver exogenous molecules noninvasively into a specific target site. In this study, we evaluated the application of this technology to cancer gene therapy using prodrug activation therapy. Low-intensity pulsed ultrasound (1 MHz; 1.3 W/cm^2) and NBs were used to transduce the herpes simplex thymidine kinase (HSV*tk*) gene *in vitro*, leading to gene transfer. The addition of ganciclovir (GCV) to the transduced cells led to HSV*tk*/GCV-dependent cell death mediated by apoptosis. This technology was then assessed *in vivo*, using mice bearing subcutaneous tumors (1 MHz; 3.0 W/cm^2). Gene transfer to the tumor, measured by luciferase activity, was transient, with a peak of expression 24 h after transduction, and decreased at 48 h, demonstrating the transient nature of US/NB-mediated gene transfer. The therapeutic potential of this approach was evaluated through repeated intratumoral gene delivery using US/NB-mediated transfer of the HSV*tk* gene, followed by recurrent administration of GCV, using two different experimental treatment protocols. In both cases, dramatic reductions of the tumor size by a factor of four were observed. Altogether, these data demonstrate the potential of US/NB as a new physical gene delivery method for cancer gene therapy. (E-mail: kodama@tubero.tohoku.ac.jp) © **2008 World Federation for Ultrasound in Medicine & Biology.**

Key Words: **Membrane permeability, *In-vivo* imaging, Molecular delivery, Cancer gene therapy.**

INTRODUCTION

Cancer therapy based on gene delivery requires highly efficient molecular delivery methods into a specific target site. One of the physical methods of gene delivery exploits nano/microbubbles (NBs) combined with ultrasound (US). Nano/microbubbles are encapsulated gas bubbles with a radius of <5 μm. The shell membrane consists of albumin, lipid or polymer. The inside gas comprises either air or perfluorocarbons (large molecules have a small diffusion efficiency into liquid, resulting in increased bubble life time) (Chomas et al. 2001; Harvey et al. 2001). These bubbles are not only used as US contrast agent to identify and delineate cardiac anatomy, such as thrombi or clot formation, but they are also used for evaluation of blood pool and blood flow at the microvascular level (Lindner 2004). The mechanical index (MI, defined as the peak negative pressure divided by the square root of the US frequency) of US used in clinical application is 0.05 to 1.9 (McCulloch et al. 2000) and NBs collapse at MI = 0.3 to 0.5 (Ammi et al. 2006; Chen et al. 1995; Wu and Tong 1998). The impulsive pressures generated by either the collapse of NBs or cavitation bubbles created by the collapse of NBs are able to induce a transient permeabilization of cells, followed by the entry of exogenous molecules into cells. This method is not toxic and nonimmunogenic and can be combined with chemotherapy (Pitt et al. 2004).

Suicide gene therapy involves transfer into cancer cells of a gene capable of converting nontoxic prodrugs into cytotoxic drugs. One of the most common approaches uses the herpes simplex virus thymidine kinase (HSV*tk*) gene combined with the prodrug ganciclovir (GCV). The nucleoside analogue GCV is phosphorylated 1,000 times less efficiently by eukaryotic thymidine kinases and experimentally, *in vivo*, GCV is only phosphorylated by cells producing the virus enzyme HSV*tk*

Address correspondence to: Tetsuya Kodama, Ph.D., Professor, Biomedical Engineering Research Organization, Tohoku University, 2–1 Seiryo-machi, Aoba-ku, Sendai 980–8575, Japan. E-mail: kodama@tubero.tohoku.ac.jp

(Keller et al. 1981; Oliver et al. 1985). The product of the reaction (GCV-MP) is then further phosphorylated to GCV-diphosphate (GCV-DP) and GCV-triphosphate (GCV-TP) by endogenous cellular kinases. GCV-TP inhibits competitively the incorporation of dGTP into DNA (Mesnil and Yamasaki 2000), resulting in cell death (Fillat et al. 2003; Mesnil and Yamasaki 2000). Apoptosis has been suggested to be involved in the cell death, which may occur by a pathway independent of p53 (Wallace et al. 1996). In fact, it has been reported that cell lines with mutant p53 expressing HSV*tk* were not resistant to GCV (Vassaux and Martin-Duque 2004; Wallace et al. 1996; Yoon et al. 1999). Cytotoxicity is observed not only in HSV*tk*-positive cells but also in neighboring HSV*tk*-negative cells as a result of the bystander effect. HSV*tk*-negative cells show cytotoxicity *in vitro* when the population of cultured cells contained only 10% HSV*tk*-positive cells (Freeman et al. 1993). This bystander effect is regarded as a transfer phenomenon of the toxic metabolites of GCV from HSV*tk*-positive cells to HSV*tk*-negative cell, in which gap junctional intercellular communication (GJIC) appears crucial.

In the present report, we evaluated the potential of US and NBs as a physical method of gene transfer in cancer gene therapy using the HSV*tk*/GCV system as a therapeutic agent.

MATERIALS AND METHODS

Nano/microbubbles

Two types of NBs, Optison™ (Amersham Health PLC, Oslo, Norway) and lipid-micelle bubbles were used. Both bubbles provided very similar physical chemical properties (size distribution and ζ potential). A report on the systematic comparison of the two reagents is currently in preparation. Optison is an octafluoropropane (C_3F_8)-filled albumin microspheres that has a mean diameter between 3.0 and 4.5 μm (max. 32.0 μm). In this study, the mean concentration was set to the arithmetic average of 6.5×10^8 bubbles/mL. Lipid-micelle bubbles were created in an aqueous dispersion of 2 mg/mL 1,2-distearoyl-sn-glycero-3-phosphocholine (DSPC) (Avanti Polar Lipids, Alabaster, AL, USA) and 1 mg/mL polyethleneglycol-40 stearate (PEG) (Sigma-Aldrich Co., St. Louis, MO, USA) using a 20-kHz sonicator (Vibra Cell, Sonics & Materials, Inc., Danbury, CT, USA) in the presence of C_3F_8 gas (Aoi et al. 2006). The theoretically calculated concentration was 1.6×10^{10} bubbles/mL. The lipid bubble surface that comprised lipid molecules was confirmed by staining lipid molecules with 3 μM FM1–43 (553 nm, Abs: 570 nm, Em., Molecular Probe Inc, Eugene, OR, USA) under an inverted microscope (IX81, Olympus Co., Tokyo, Japan). The bubble size distribution was determined by using a laser diffraction particle size analyzer (particle range of 0.6 nm–7 μm, ELSZ-2, Otsuka Electronics Co. Ltd, Osaka, Japan). The peak diameters expressed in terms of the size distribution of Optison and lipid bubbles were 1689 $\pm$ 150 nm (n = 4) and 1272 $\pm$ 163 nm (n = 7), respectively. Because the volume distribution is proportional to the third power of the size, the peak of the size distribution tends to be measured as a smaller value than that of the volume distribution. The ζ potential of the bubbles was measured by the ELSZ-2 in phosphate-buffered saline without Mg_{2+} and Ca_{2+} (PBS). Zeta potential refers to the electrostatic potential generated by the accumulation of ions at the surface of a bubble that is organized into an electrical double layer. The ζ potential of the Optison and lipid bubble, was –36.9 $\pm$ 2.70 mV (n = 3) and –4.11 $\pm$ 0.74 mV (n = 4), respectively, indicating that Optison have larger mutual impulsive forces and higher stability compared with the lipid bubbles. In our previous experiments, there were no significant differences in *in-vitro* gene activity between Optison and lipid micelle bubbles (data not shown). In the following experiments, lipid-micelle bubbles and Optison were used for *in-vitro* and *in-vivo* experiments, respectively.

Cell preparation

Human lung carcinoma (A549) and murine colon carcinoma (colon26, which was abbreviated as C26 in the text) were obtained from the Cell Resource Center for Biomedical Research, Institute of Development, Aging and Cancer, Tohoku University, Sendai, Japan. Murine breast carcinoma (EMT6) cells were obtained from the American Type Culture Collection (Manassas, VA, USA). Murine breast carcinoma cells (EMT6-luc) stably expressing the firefly luciferase gene were prepared by transfected pEGFPLuc (BD Biosciences, Franklin Lakes, NJ, USA) and Lipofectin Transfer Reagent (Invitrogen, Carlsbad, CA, USA). Human colon carcinoma cells (HT29) were obtained from Cancer Research UK (London, UK), and human colon carcinoma cells (HT29-luc) stably expressing the firefly luciferase gene were obtained from Xenogen (Alameda, CA, USA). A549, C26, HT29 and HT29-luc cells were cultured under standard conditions in RPMI 1640 supplemented with 10% heat-inactivated fetal bovine serum (FBS) (Invitrogen) and 1% L-glutamine-penicillin-streptomycin (Sigma-Aldrich, St. Louis, MO, USA), whereas EMT6 cells and EMT6-luc were cultured in DMEM (Sigma-Aldrich) medium with the same supplements. Cells cultured in a 10-cm culture dish were maintained in a humidified incubator at 37° C under an atmosphere of 5% CO_2 and 95% air.

Plasmids

The luciferase reporter vector pGL3-control (Promega, Madison, WI, USA), which expresses luciferase from SV40 promoter, pGV24 vector in which HSV*tk* expression is driven by the ERBB2 promoter (Vassaux et al. 1999) and pRS303 that does not have any transgene expressed, were used as mock plasmid. pGV24 and pRS303 were referred to as pHSV*tk* and pMock, respectively.

Ultrasound

Two 1-MHz submersible US probes (Fuji Ceramics Co., Fujinomiya, Japan), 12 and 38 mm in diameter, were used for *in-vitro* and *in-vivo* experiments, respectively. Each probe was located in a test chamber (380 × 250 × 130 mm^3) filled with tap water. Each frequency was generated by a multifunction synthesizer (WF1946A; NF Co., Yokohama, Japan), amplified with a high-speed bipolar amplifier (HSA4101; NF Co.). The pressure values were measured by a PVDF needle-hydrophone (PVDF-Z44–1000; Specialty Engineering Associates, Soquel, CA, USA) at a stand-off distance of 1 mm from the transducer surface using a stage control system (Mark-204-MS, Sigma Koki, Tokyo, Japan). The signals from both the amplifier and the hydrophone were recorded into a digital phosphor oscilloscope (Wave Surfer 454, 500 MHz, 1 mol/LΩ (16 pF), LeCroy Co., Chestnut, NY, USA).

In-vitro *transfection by ultrasound and nanobubbles*

In-vitro studies were performed in accordance with the Tohoku University ethical guidelines. A549 (1 × 10^4 cells/well), HT29 (1 × 10^4 cells/well), C26 (2 × 10^4 cells/well) and EMT6 (2 × 10^4 cells/well) cells were seeded in 24-well plates in complete media at 37° C in a 5% CO_2 incubator. The next day, the medium was replaced with fresh media (200 μL), containing pMock (4 μg/mL) or pHSV*tk* (4 μg/mL) with and without NBs (10% v/v). The 24-well plates were located just above the US probe in a test chamber filled with tap water and exposed to the optimized US (intensity: 1.3 W/cm^2, duty ratio: 50%, number of pulse: 2000, exposure time: 10s). The surface of the media was disturbed by US, thus we ignored the effect of standing waves on gene expression. Because cells were seeded into wells alternately, neighboring wells were not exposed to ultrasound at the same time. The plates were incubated for 1 h at 37° C in a 5% CO_2 incubator, supplemented with 800 μL of complete media and then incubated for another 24 h at 37° C in a 5% CO_2 incubator.

In-vitro *sensitivity to GCV assays*

Twenty-four hours after transfection, the media was replaced with complete media (1 mL) containing GCV (0.1–1000 μg/mL, molecular weight 255.2; F. Hoffman-La Roche Ltd., Basel, Switzerland). The plates were incubated for another three to five days at 37° C in a 5% CO_2 incubator. Survival fractions were measured by MTT assay (Kodama et al. 2003; Martinico et al. 2006). Each experiment consisted of six to 15 samples receiving US + NB + GCV with HSV*tk* (or Mock) and six to 15 control samples receiving US and NB. For each experiment, the mean % of treated samples was divided by the mean % of control samples to give a survival fraction. The mean of six to 15 survival fractions was calculated for each condition. The survival fraction of each cell line was measured at the GCV concentration where the highest statistical significant was obtained.

RT-PCR

The total RNAs were reverse-transcribed using the RNA PCR Kit (AMV) (Takara Bio Inc., Tokyo, Japan) according to the manufacturer's instructions (1 μg of total RNA was used). The cDNAs obtained were then subjected to polymerase chain reaction (PCR) amplification (3 min at 94 °C, and 35 cycles of denaturation 95 °C for 60 s, annealing 58.4 °C for 60 s and extension 72 °C for 60 s, followed by 5 min of extension 72 °C) with either HSV*tk*-specific primers (5′-AACAATGGGCATGCCTTATGC-3′; 5′-TTATACAGGTCGCCGTTGGGG-3′, with an expected PCR product of 540 bp) or β-actin–specific primers (5′-CTGTCTGGCGGCACCACCAT-3′; 5′-GCAACTAAGTCATAGTCCGC-3′, with an expected PCR product of 254 bp). The PCR products were then separated on a 2% agarose gel.

Apoptotic assay

Apoptotic cells were detected by fluorescence microscopy (DAPI staining) and TUNEL assay. For DAPI staining, cells incubated in the presence of GCV (10 μg/mL) for 24 h after the treatment of US+NB+ HSV*tk* were stained with DAPI solution (100 ng/mL). For TUNEL assay, cells were harvested at 48 h after treatment, fixed in 4% (w/v) paraformaldehyde with PBS and then washed with PBS and stored in 70% ethanol at –20° C for at least 30 min. The ethanol solution was subsequently removed after centrifugation, and cells were treated with the enzyme terminal deoxynucleotidyl transferase and FITC-labeled dUTP using the Mebstain apoptosis kit from MBL (Nagoya, Japan) according to the manufacturer's protocol. FITC-labeled cells were measured by flow cytometry (FACSCalibur, Becton Dickinson, San Jose, CA, USA). A total of 10,000 events per sample were collected in list mode, and data were analyzed with Cell Quest software (Becton Dickinson). Fluorescence data were collected by using 488-nm excitation from a 15-mW air-cooled argon-ion laser. The emission was collected through a 530 ± 30-nm band-pass